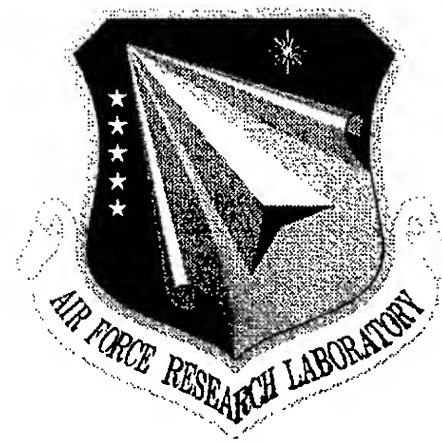


**AFRL-SN-RS-TR-2001-13**

**In-House Report**

**February 2001**



# **DISPERSION AND NONLINEARITY CHARACTERIZATION OF A MODE-LOCKED ERBIUM-DOPED FIBER LASER**

**James A. Louthain and Michael J. Hayduk**

*APPROVED FOR PUBLIC RELEASE; DISTRIBUTION UNLIMITED.*

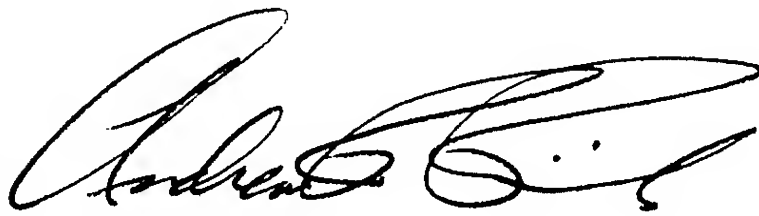
**AIR FORCE RESEARCH LABORATORY  
SENSORS DIRECTORATE  
ROME RESEARCH SITE  
ROME, NEW YORK**

**20010316 103**

This report has been reviewed by the Air Force Research Laboratory, Information Directorate, Public Affairs Office (IFOIPA) and is releasable to the National Technical Information Service (NTIS). At NTIS it will be releasable to the general public, including foreign nations.

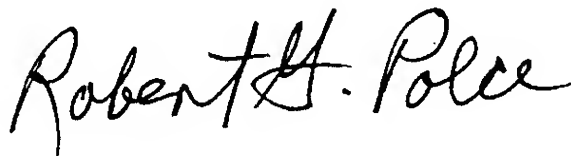
AFRL-SN-RS-TR-2001-13 has been reviewed and is approved for publication.

APPROVED:



ANDREW R. PIRICH  
Chief, Photonics Technology Branch  
Sensors Directorate

FOR THE DIRECTOR:



ROBERT G. POLCE  
Chief, Rome Operations Office  
Sensors Directorate

If your address has changed or if you wish to be removed from the Air Force Research Laboratory Rome Research Site mailing list, or if the addressee is no longer employed by your organization, please notify AFRL/SNDP, 25 Electronic Parkway, Rome, NY 13441-4515. This will assist us in maintaining a current mailing list.

Do not return copies of this report unless contractual obligations or notices on a specific document require that it be returned.

REPORT DOCUMENTATION PAGE			Form Approved OMB No. 0704-0188	
Public reporting burden for this collection of information is estimated to average 1 hour per response, including the time for reviewing instructions, searching existing data sources, gathering and maintaining the data needed, and completing and reviewing the collection of information. Send comments regarding this burden estimate or any other aspect of this collection of information, including suggestions for reducing this burden, to Washington Headquarters Services, Directorate for Information Operations and Reports, 1215 Jefferson Davis Highway, Suite 1204, Arlington, VA 22202-4302, and to the Office of Management and Budget, Paperwork Reduction Project (0704-0188), Washington, DC 20503.				
1. AGENCY USE ONLY (Leave blank)		2. REPORT DATE FEBRUARY 2001	3. REPORT TYPE AND DATES COVERED In-House, 1 Oct 99 - 30 Sep 00	
4. TITLE AND SUBTITLE  DISPERSION AND NONLINEARITY CHARACTERIZATION OF A MODE-LOCKED ERBIUM-DOPED FIBER LASER			5. FUNDING NUMBERS  PE - 62204F PR - PADC TA - SN WU- 01	
6. AUTHOR(S)  James A. Louthain and Michael J. Hayduk				
7. PERFORMING ORGANIZATION NAME(S) AND ADDRESS(ES)  Air Force Research Laboratory/SNDP 25 Electronic Parkway Rome, NY 13441-4515			8. PERFORMING ORGANIZATION REPORT NUMBER  AFRL-SN-RS-TR-2001-13	
9. SPONSORING/MONITORING AGENCY NAME(S) AND ADDRESS(ES)  Air Force Research Laboratory/SNDP 25 Electronic Parkway Rome, NY 13441-4515			10. SPONSORING/MONITORING AGENCY REPORT NUMBER  AFRL-SN-RS-TR-2001-13	
11. SUPPLEMENTARY NOTES  AFRL Program Manager: Michael J. Hayduk/SNDP/(315)330-7753.				
12a. DISTRIBUTION AVAILABILITY STATEMENT  APPROVED FOR PUBLIC RELEASE; DISTRIBUTION UNLIMITED.			12b. DISTRIBUTION CODE	
13. ABSTRACT (Maximum 200 words)  This report describes the results of dispersion and nonlinearity experiments of the components required for the development of picosecond passively mode-locked fiber lasers. First, we will summarize the interferometric dispersion measurement technique and results for short lengths of fiber (< 1 meter). We measured dispersion of standard fiber at 16.9 +/- 1.4 ps/nm and Er-doped fiber at 8.5 +/- 1.6 ps/nm at 1550 nm. Next, we measured the group delay of three chirped Bragg gratings using a phase difference method and a tunable laser. These chirped Bragg gratings served as one of the mirrors in the linear fiber laser cavity. Finally, we measured the nonlinearity of five different multiple quantum well saturable absorbers using a z-scan technique. The saturable absorbers served as the mode-locking mechanism in the passively mode-locked fiber laser. The values of the nonlinear absorption ranged from 1 to 3 cm/W. We also measured the refractive nonlinearity of one of the MQW saturable absorbers to be about -4 x 10 cm/W.				
14. SUBJECT TERMS optical dispersion, optical fiber lasers, mode-locked lasers, rare-earth materials/devices, optical nonlinearity, multiple quantum wells, saturable absorber			15. NUMBER OF PAGES 36	
			16. PRICE CODE	
17. SECURITY CLASSIFICATION OF REPORT  UNCLASSIFIED	18. SECURITY CLASSIFICATION OF THIS PAGE  UNCLASSIFIED	19. SECURITY CLASSIFICATION OF ABSTRACT  UNCLASSIFIED	20. LIMITATION OF ABSTRACT  UL	

## Table of Contents

<u>Section</u>	<u>Page</u>
Preface	ii
1. Introduction	1
2. Dispersion measurements of erbium-doped optical fiber	3
3. Dispersion measurements of chirped fiber Bragg gratings	9
4. Nonlinearity measurements of multiple quantum well saturable absorbers	12
5. Conclusions	17
6. References	19
7. Acknowledgements	20
Appendix	21
I Dispersion Calculation_linear.vi	21
II Sweep Phase Wavelength.vi	23
III z-scan.vi	25

## **Preface**

The three measurement systems were developed and built by J. Louthain. M. Hayduk and R. Bussjager built and characterized the fiber lasers. J. Haus developed the mode-locked laser model used to simulate the performance of the fiber lasers.

## 1. Introduction

Mode-locked erbium-doped fiber lasers are inexpensive compact sources of ultrashort pulses in the 1.55  $\mu\text{m}$  wavelength regime. Ultrashort pulse sources have many potential applications including high-repetition-rate sources for telecommunications, local area networks, or RF digitization. Recent advances have been made in photonic analog to digital conversion.[1] Many passive mode-locking techniques have been presented in the past operating both in normal and anomalous dispersion regimes. Recently semiconductor saturable absorbers in the form of bulk, multiple quantum well (MQW) or single quantum well – saturable Bragg reflector (SBR) have been used to mode-lock linear fiber cavities [2-7]. Complex Ginzburg-Landau equations have also been used to model mode-locked laser operation successfully [3, 5]. In particular, Kutz et. al. and Haus et. al. made a direct comparison between simulations and experimental results on a fiber laser.[3, 5] The dispersion and nonlinearity of the components can be used to accurately model the cavity.

In this paper we present measurements of components of a fiber laser mode-locked by MQW saturable absorber. Our cavity is high loss and its non-linear dynamics are dominated by the saturable absorber. The construction of our compact, polarization insensitive, passively erbium-doped fiber laser employing a MQW saturable absorber and a chirped fiber Bragg grating is shown in Figure 1. This is a high loss cavity with an estimated 60 % loss per round trip. The measured typical autocorrelation and optical spectrum of the fiber laser is shown in Figure 2.[5,8]

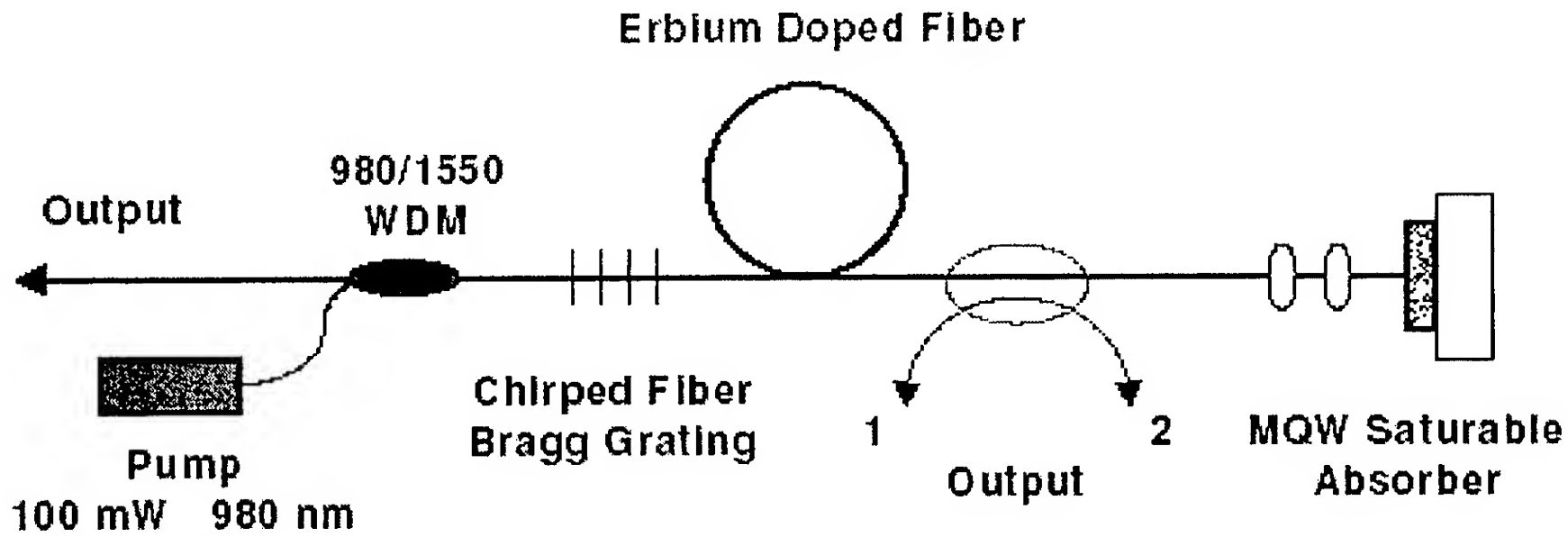


Fig. 1. Schematic diagram of the laser cavity. Outputs "1" and "2" are used to characterize the laser, but the normal output is on the left.

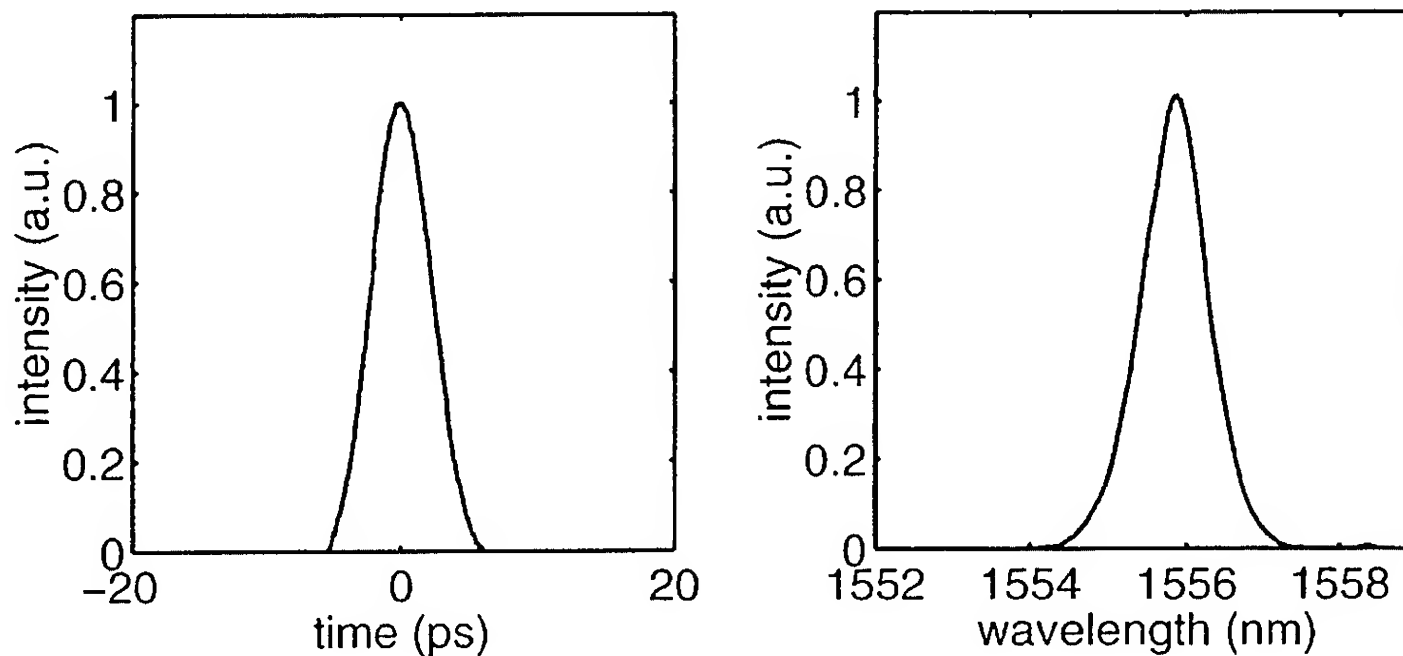


Fig. 2. Autocorrelation spectrum (3.4 ps pulse width) and optical spectrum (0.92 nm spectral width) of output pulses from the laser cavity.

We measured the dispersion of the fiber and Bragg gratings as well as the non-linearity of the MQW saturable absorber. Dispersion of optical fiber has become an essential performance factor, as bit rates and spectral bandwidths increase in telecommunication applications. Precise dispersion information is also important in designing ultra-fast optics. The nonlinearity of the saturable absorber is substantial since the structure contains 50-75 periods of 100 Å InGaAs 100

Å InAlAs layers. This large saturation of absorption nonlinearity was required to overcome the high loss of the cavity. Unfortunately, large refractive nonlinearity accompanies the absorption nonlinearity. The dispersion in the chirped fiber Bragg grating was used in the laser to compensate for the large refractive nonlinearity of the saturable absorber.[8] Precise dispersion management is required for stable mode-locked operation.[ 5-7]

The work performed in the measurement of mode-locked fiber laser components can be summarized by three efforts:

1. We developed a measurement system to characterize the dispersion of optical fiber. We use spectral interference to measure the dispersion of fiber lengths of less than 1 meter to within 0.1-picosecond-resolution.
2. We built a measurement system to characterize the dispersion of optical fiber chirped Bragg gratings. We measured the dispersion of chirped Bragg gratings using a phase-shift measurement technique.
3. We investigated the nonlinearity of the multiple quantum well saturable absorber. The z-scan technique was performed on the saturable absorber to determine both the refractive and absorptive nonlinearity.

## **2. Dispersion measurements of erbium-doped optical fiber**

We used a balanced Michelson interferometer and a broad-band LED, 60nm full-width-half-maximum (FWHM), centered at 1540 nm to measure the dispersion of the actual fiber used in the laser cavity. Often times dispersion in a small piece of fiber ( $< 1$  m) can differ significantly from the average value of the entire spool. In addition, high-loss erbium and ytterbium-doped fiber cannot be measured by conventional time-of-flight measurements. Using



this method, we were able to measure the linear dispersion of less than a half meter of fiber down to as low as 4 fs/nm. The experimental setup is shown in Figure 3. One arm of the interferometer includes the fiber length used within the cavity and the other arm is a variable free-space section. The light travels through one port of the 3-dB coupler and reflects off the broad-band mirrors in each arm.[9]

The following interference spectrum was collected at the other port and measured by the optical spectrum analyzer

$$I = I_{fs}^2 + I_{de}^2 + 2I_{fs}I_{de} \cos(\phi(\omega)), \quad (1)$$

where

$$\phi(\omega) = \beta_{fs}(\omega)d - \beta_{de}(\omega)L, \quad (2)$$

$I_{fs}$ ,  $I_{de}$ ,  $\beta_{fs}$ , and  $\beta_{de}$  are the respective intensities and propagation constants for the free space and dispersive element arms,  $\omega$  is the optical angular frequency,  $d$  is the length of the free space arm, and  $L$  is the length of the dispersive element arm.[4,9,11]

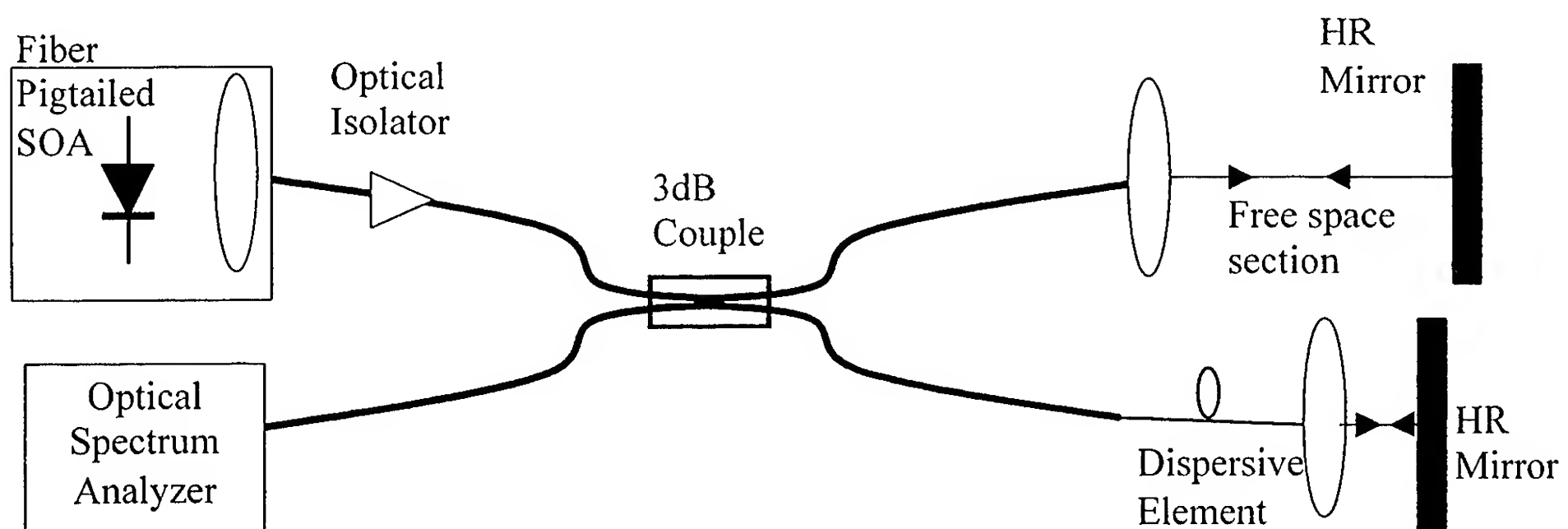


Figure 3. Schematic of Michelson interferometer used to measure dispersion of optical components.

If we expand  $\beta_{de}$  in a Taylor series about  $\omega = \omega_0$  corresponding to  $\lambda = \lambda_0$  and collect all constant terms into an unknown phase term  $\phi_0$ ,  $\phi(\omega)$  becomes

$$\phi(\omega) = \phi_0 + \left[ \beta_1(\omega_0)L - \frac{d}{c} \right] (\omega - \omega_0) + \frac{1}{2} \beta_2(\omega_0)L(\omega - \omega_0)^2 + \frac{1}{6} \beta_3(\omega_0)L(\omega - \omega_0)^3 + \dots, \quad (3)$$

where  $\phi_0$  is a constant,  $c$  is the speed of light,  $\beta_2$  is the total group velocity dispersion, and  $\beta_3$  is the third order dispersion of the fiber under test.[4,9,11] We neglect terms higher than third order. Adjusting the free space arm until  $\beta_1(\omega_0)L = d/c$  makes the second term drop out, leaving the second order and higher terms.

The wavelength point of symmetry where the phase shift through the free-space path is the same as the fiber path occurs at  $\lambda = \lambda_0$ . Adjusting the free-space pathlength will tune the interferometer to different wavelength symmetry points. For instance, the wide center peak in Figure 3 corresponds to this symmetry point where  $\lambda = \lambda_0$ . Also, from this adjustment one can determine the sign of the dispersion. If increasing the free-space path causes the symmetry point to move to higher wavelengths, the  $\beta_2(\omega_0)$  term will be negative. If the symmetry point moves to lower wavelengths, the  $\beta_2(\omega_0)$  dispersion term will be positive.

The interference spectrum at the output port contains nulls where  $\phi(\omega) = (2n+1)\pi$  and peaks where  $\phi(\omega) = 2n\pi$  as shown in Figure 4. We can now write Eq. (3) in the following form for the peaks in the interference pattern:

$$F_N = \phi_0 + \frac{L}{2} \beta_2 \left[ \frac{2\pi c}{\lambda_N} - \frac{2\pi c}{\lambda_0} \right]^2 + \frac{L}{6} \beta_3 \left[ \frac{2\pi c}{\lambda_N} - \frac{2\pi c}{\lambda_0} \right]^3 - 2\pi N = 0 \quad (4)$$

where  $\lambda_0$  is the symmetry point in wavelength,  $N$  is the peak location, and  $\lambda_N$  is the wavelength of the corresponding peak.[10] We set up a system of simultaneous equations for the three unknowns  $\phi_0$ ,  $\beta_2$ , and  $\beta_3$ . Each equation corresponds to a maximum (or minimum) of the

interference pattern spectrum with the corresponding value of  $N$ . The dispersion can be expressed as delay time dispersion,  $D$ , in units of ps/nm-km using the following relationship

$$D = -\frac{2\pi c}{\lambda_0^2} \beta_2, \quad (5)$$

where  $\beta_2$  is the group velocity dispersion,  $c$  is the speed of light, and  $\lambda_0$  is the wavelength.[6]

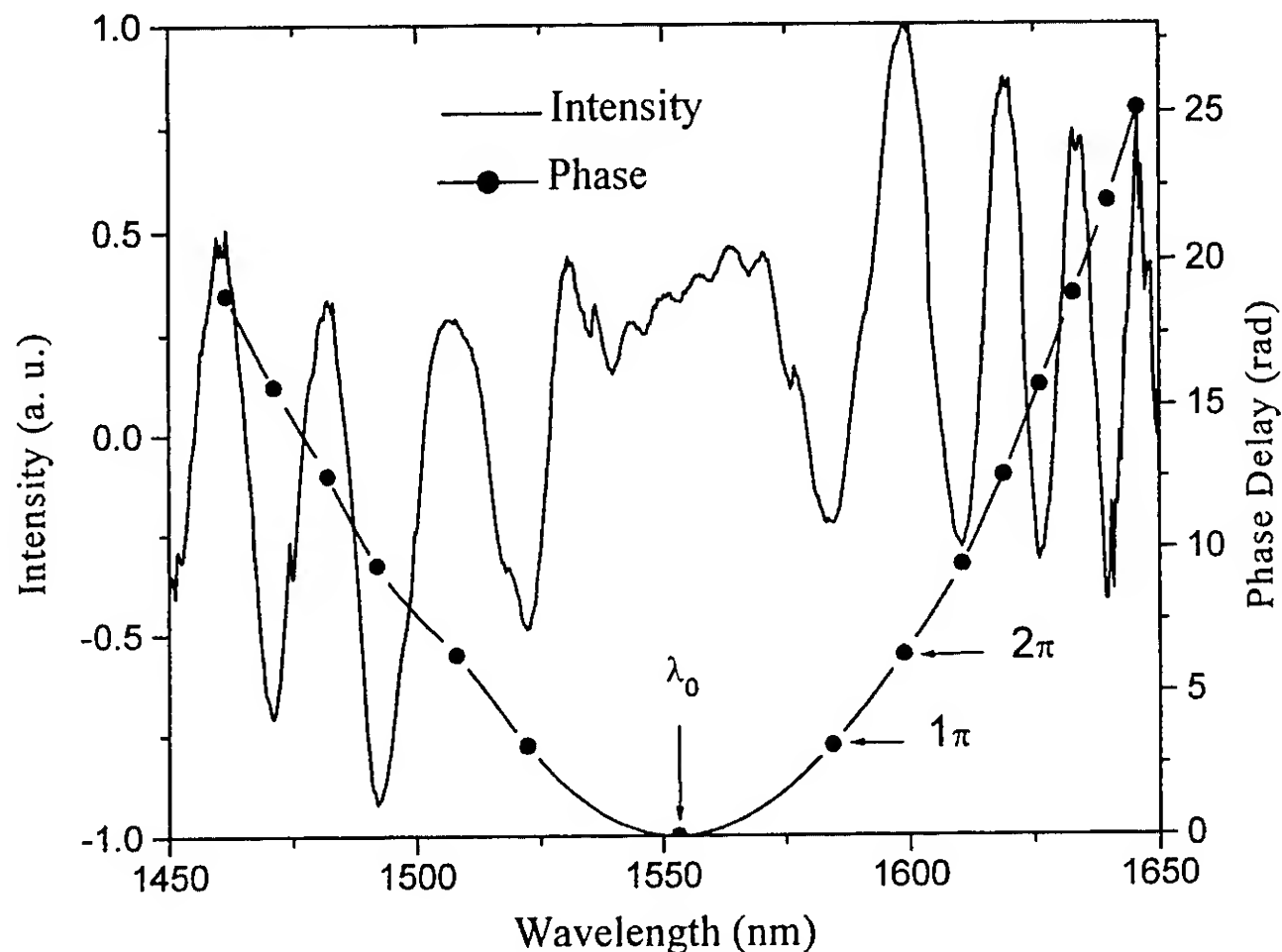


Figure 4. Typical interference spectrum measured by the optical spectrum analyzer. The associated phase is plotted on the right axis by locating the peaks and valleys and assigning the appropriate phase.

Using the setup in Figure 3, we measured the dispersion of standard single mode fiber and erbium-doped fiber. We used data acquisition and instrument control and a PC running appropriate software to solve Eq. (4) automatically. See Appendix I for the Labview™ program. This automation allowed us to take several readings. The dispersion of standard single mode fiber is published as approximately

$$D(\lambda) \approx \frac{S_0}{4} \left[ \lambda - \frac{\lambda_0^4}{\lambda^3} \right] \text{ ps/nm-km, for } 1200 \text{ nm} \leq \lambda \leq 1600 \text{ nm,} \quad (6)$$

where  $\lambda$  is the operating wavelength,  $\lambda_0$  is the zero dispersion wavelength, and  $S_0$  is the zero dispersion slope.[13] Typical values are  $1301.5 \text{ nm} \leq \lambda_0 \leq 1321.5 \text{ nm}$  and  $S_0 \leq 0.092 \text{ ps/nm-km}$ . We used the typical value of  $0.90 \text{ ps/nm-km}$  for  $S_0$ . [13]

Figure 5 shows how our experimental results compare with the published dispersion of STANDARD FIBER for a 42.5-cm fiber length. At 1550 nm the dispersion is about  $16.9 \pm 1.4 \text{ ps/nm-km}$  and about  $17.6 \pm 1.4 \text{ ps/nm-km}$  at 1560 nm. Notice how our measurements diverge from the published results as we moved away from 1550 nm. Our source was centered at 1540 nm with a spectral width of 60 nm FWHM. Therefore, these variations are most likely due to low power levels in the tails of the LED spectrum.[9]

Figure 6 shows our experimental results for a 38-cm erbium-doped fiber. The power levels in the erbium-doped fiber were lower than in the standard fiber measurements due to the absorption that occurred at 1530 nm. This contributed to more fluctuation in the measurements which in turn required more data points. Again, these measurements will be more accurate around 1550 nm. At 1550 nm the dispersion is about  $8.5 \pm 1.6 \text{ ps/nm-km}$  and at 1560 nm it is about  $10.4 \pm 1.6 \text{ ps/nm-km}$ . [9]

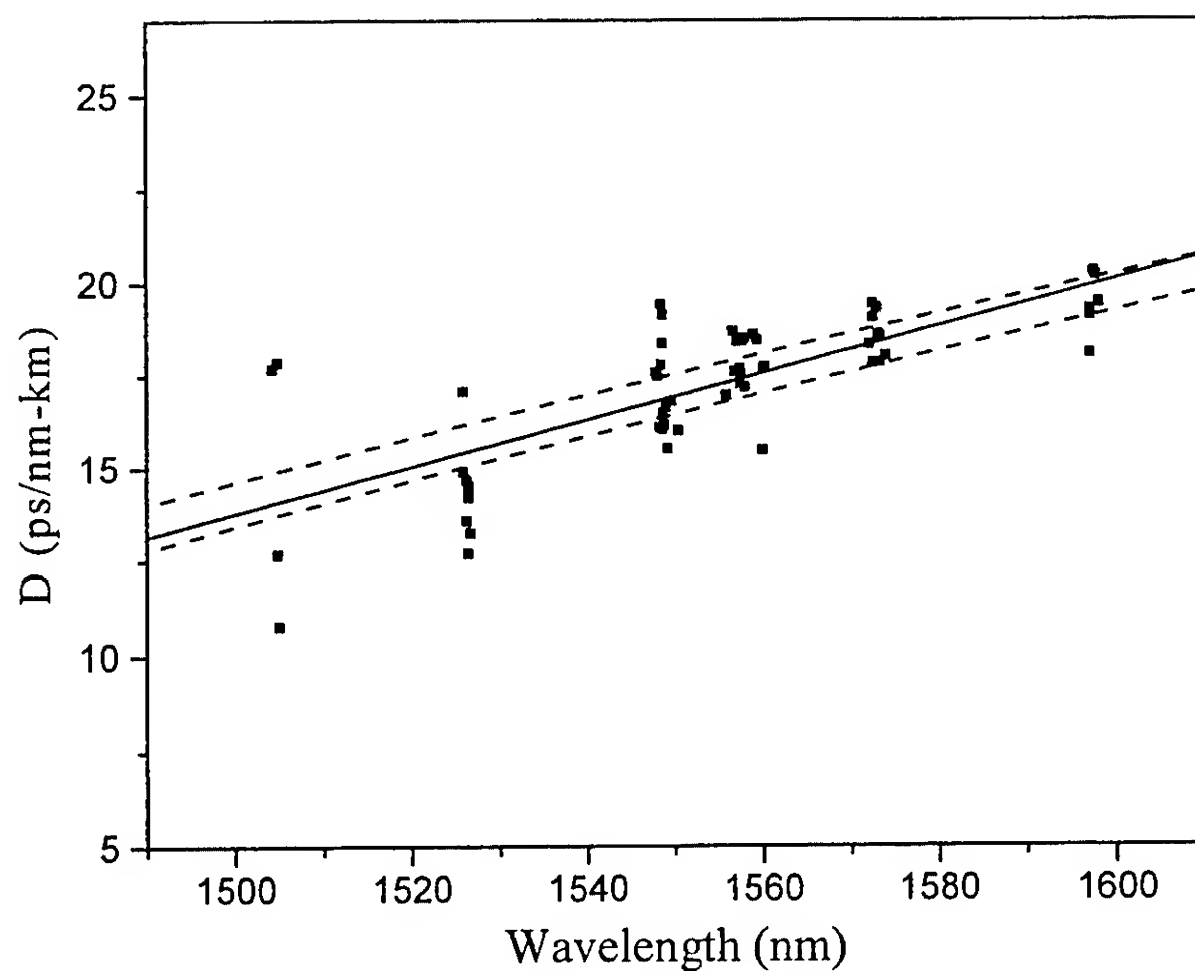


Figure 5. The squares are individual measurements of the dispersion of standard single mode fiber using the spectral interference method. The solid line is a linear fit to the data. The top and bottom dashed lines are the published dispersion specifications of standard fiber for a zero dispersion wavelength of 1301.5 nm and 1321.5 nm, respectively.

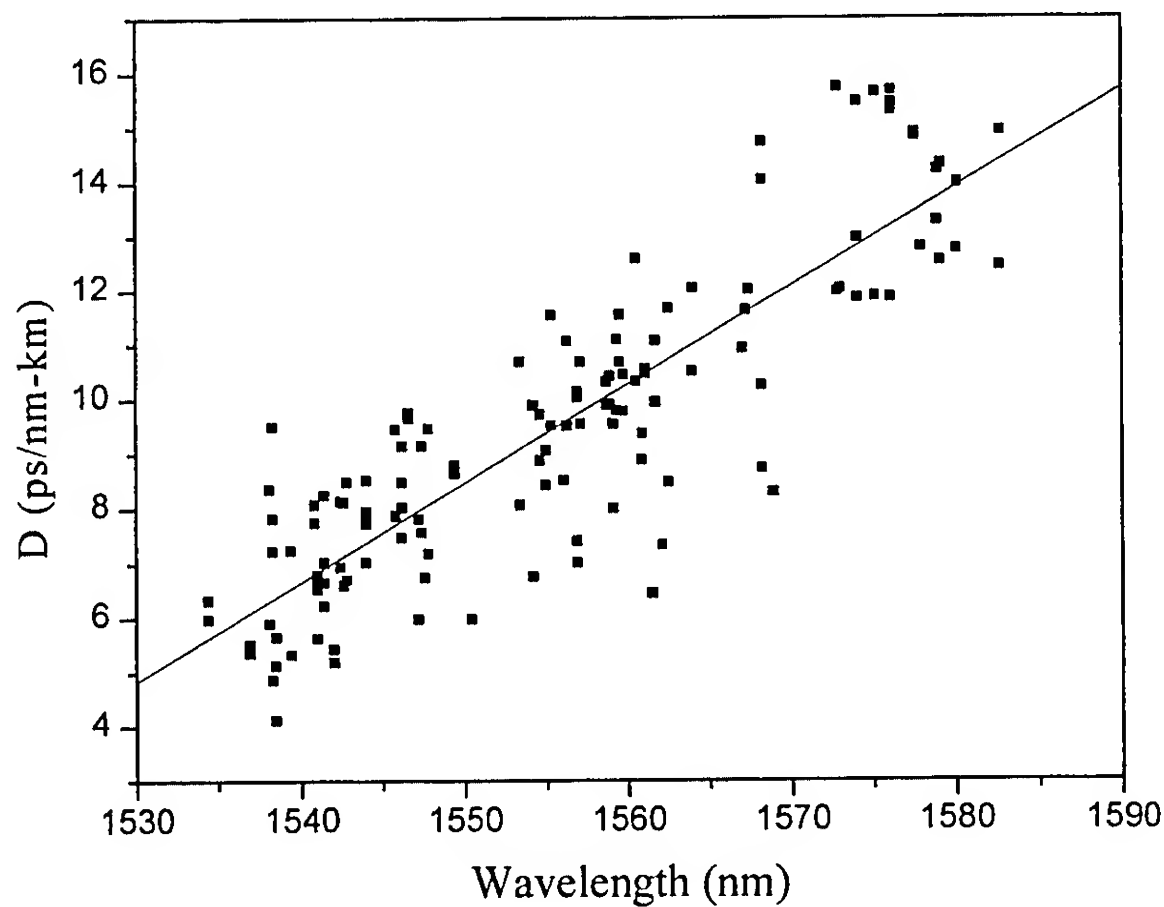


Figure 6. The squares are individual measurements of the dispersion of the erbium-doped fiber using the spectral interference method. The solid line is a linear fit to the data. The erbium-doped fiber had a concentration of about 1200 parts per million and an outside fiber diameter of about 113  $\mu\text{m}$ .

### 3. Dispersion measurements of chirped fiber Bragg gratings

The chirped fiber Bragg gratings are much more dispersive (over two orders of magnitude) than standard optical fiber. Therefore, a time-of flight type measurement is more appropriate than an interferometric technique. Our experimental setup is shown in Figure 4. In this technique, laser light is intensity modulated with an RF signal and is sent through an equal power splitting 2x2 fiber coupler (3dB coupler) to the grating mirror under test. The light reflects off the grating and travels back through the splitter to a high-speed detector. Using an HP Network Analyzer, we measure the phase shift between the signal reflected off the grating and the input RF signal. As the wavelength of the tunable laser changes the phase shift changes due to the dispersion. The phase shift is then converted to group delay versus wavelength to illustrate the dispersion.[12]

The chromatic dispersion,  $D(\lambda)$ , is obtained from the difference in the group delay at two closely spaced wavelengths. The dispersion is the average delay over the wavelength range. The resolution of the dispersion measurement is determined by the spectral width of the source. The spectral width of our tunable laser was 0.1 nm full-width-half-maximum (FWHM). Therefore, we were not able to measure the fine structure of the grating. The end fibers were angle cleaved to reduce spurious reflections from the end facets of the fibers. The following relation was used to calculate the chromatic dispersion coefficient in ps/nm:

$$D(\lambda) = 10^{12} \times \frac{[\Phi(\lambda_1) - \Phi(\lambda_2)]}{[360 \times f \times \Delta\lambda]}, \quad (7)$$

where  $\lambda = (\lambda_1 + \lambda_2)/2$ ,  $\Phi(\lambda_{1,2})$  are the measured phase shifts in degrees,  $\Delta\lambda = \lambda_1 - \lambda_2$  is the difference in nm between the two optical wavelengths, and  $f$  is the RF modulation frequency in

Hz.[12] We used a modulation frequency of 100 MHz. The following simplified relation will find the absolute group delay in picoseconds  $10^{12} \times [\Phi(\lambda)]/[360 \times f]$ . [12]

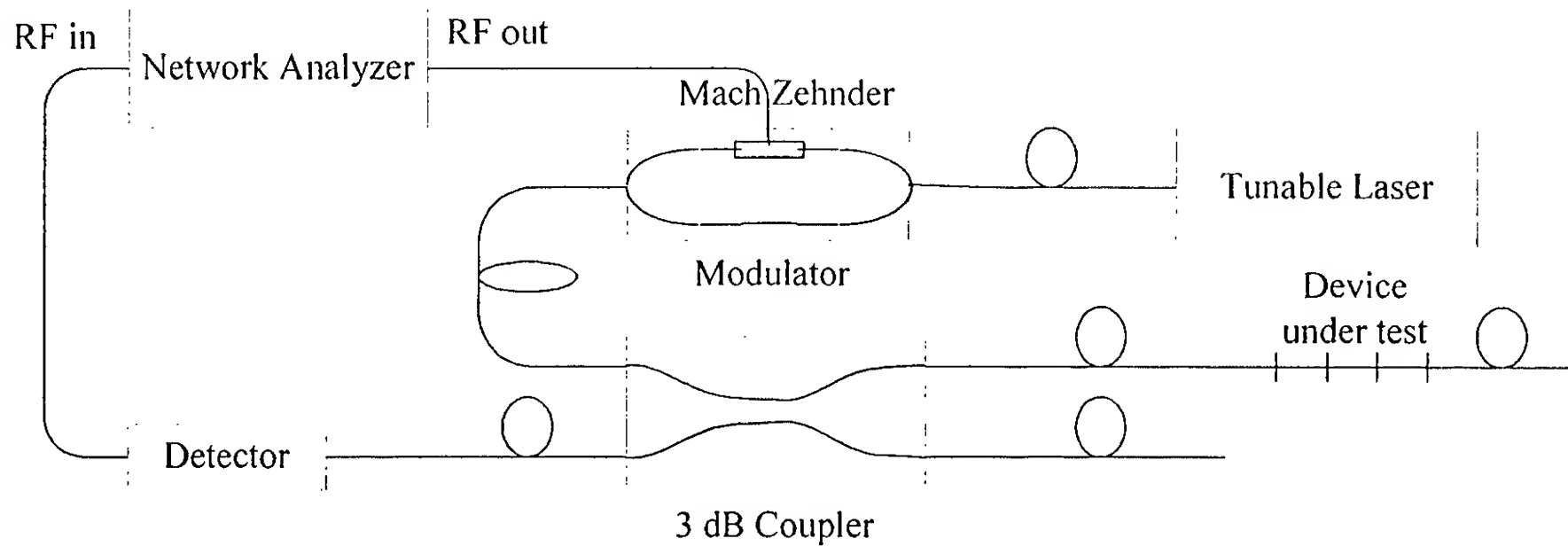


Figure 7. Setup for chromatic dispersion measurement of a reflection fiber Bragg grating.

We used the differential phase shift technique to measure the dispersion and reflection spectrums for three very different gratings. We employed data acquisition and instrument control and a PC running appropriate software to calculate the group delay. See Appendix II for the Labview™ program. Figures 8-10 show the group delays. The dispersion in ps/nm corresponds to the slope of the curve. The grating in Figure 8 is an ordinary highly reflective Bragg grating with a bandwidth of about 1.5 nm. It is very narrow with a relatively flat dispersion over the spectral width. Figure 9 shows the dispersion of a linearly chirped grating with a bandwidth of about 5.2 nm. The average slope from 1553 to 1556.5 nm is  $-10.3 \pm 0.2$  ps/nm. Finally, in Figure 10 we show the dispersion of a 10 nm wide Bragg grating. This grating was built to be a wide-band reflector without any regard for dispersion characteristics. The grating has positive dispersion below 1556 nm and negative dispersion above 1556 nm. Due to etalon effects in the tunable laser, each of these plots have oscillations with a period of about 0.35 nm.[9]

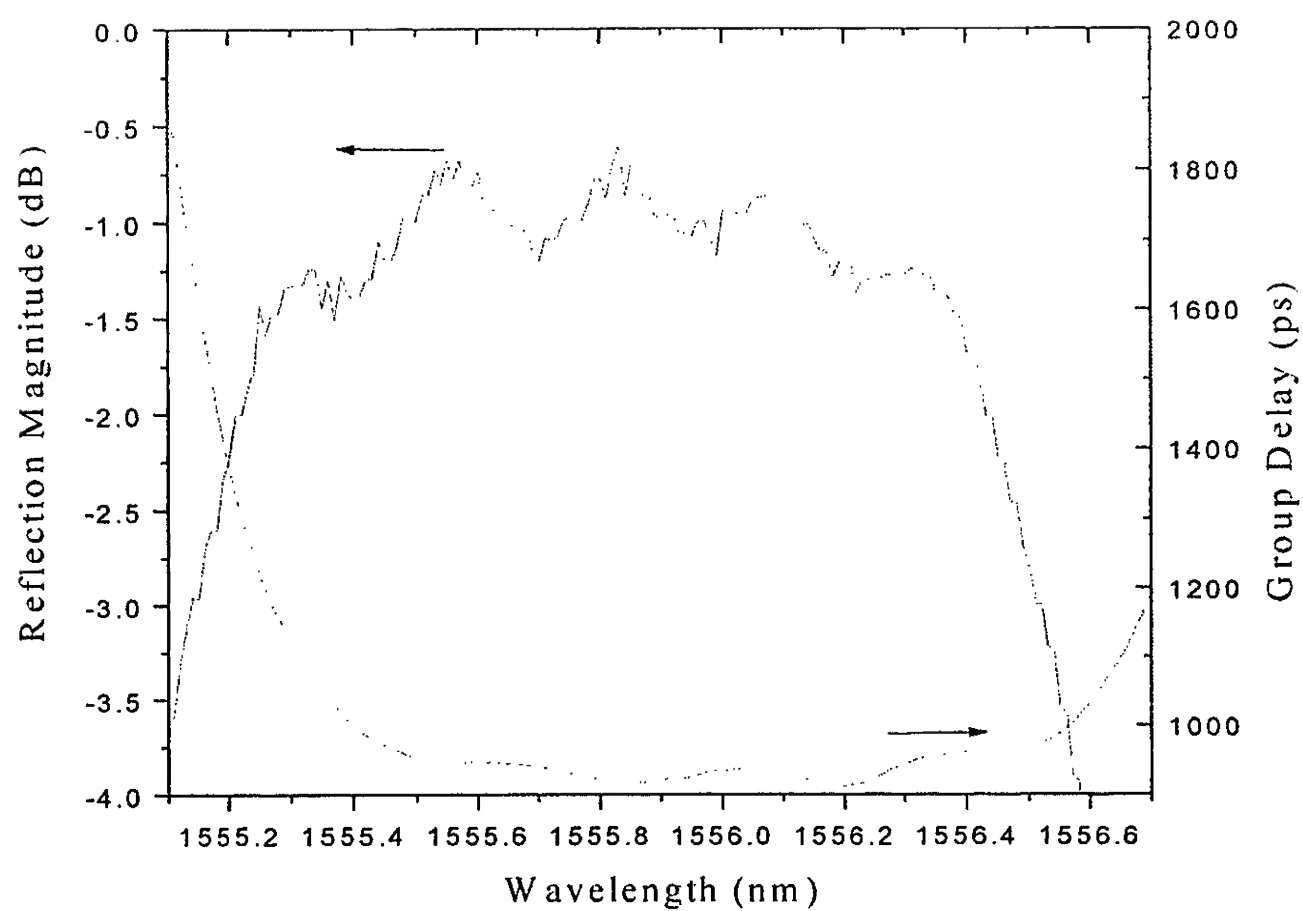


Figure 8. Reflection magnitude and group delay of a narrow-band high-reflection Bragg grating.

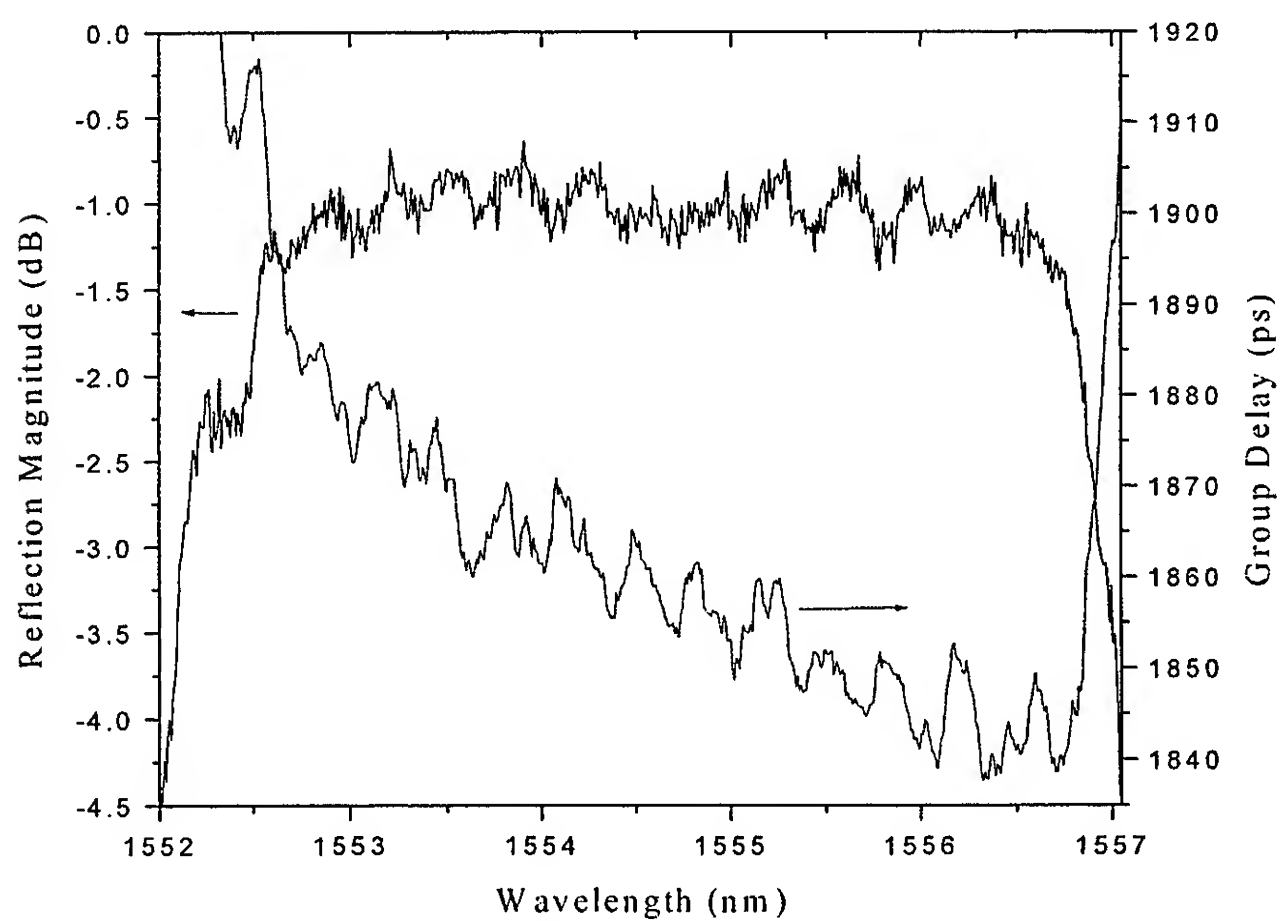


Figure 9. The reflection magnitude and group delay of a wide-band chirped grating (3M CS-98-3312 serial # 8217-7008). The slope over 1553 to 1556.5 nm is  $-10.3 \pm 0.2$  ps/nm.



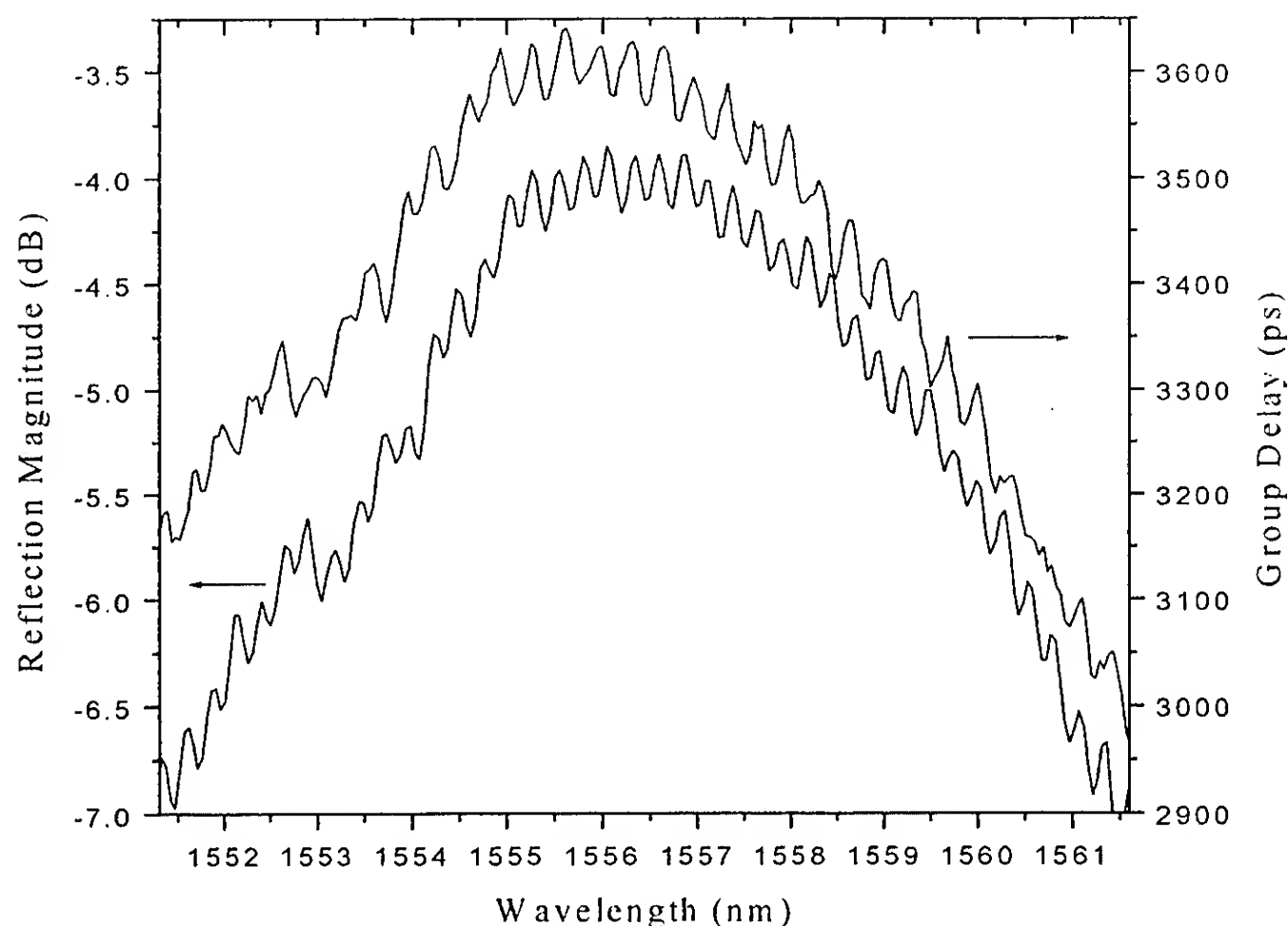


Figure 10. The reflection magnitude and group delay of a wide-band chirped grating (3M CS-96-2006 serial # 6229-1006).

#### 4. Nonlinearity measurements of multiple quantum well saturable absorbers

Next, we measured the nonlinearity of the saturable absorbers using the z-scan technique. The nonlinear absorption is the mechanism that provides the mode-locking of the laser. The refractive nonlinearity balances the dispersion within the cavity. We were able to determine the nonlinear absorption due to saturation of absorption and the refractive nonlinearity using the same experimental set-up. We determined the nonlinear absorption from an open aperture z-scan. This technique was first described by Sheik-Bahae.[15]

Our Z-scan set-up is shown in figure 11. In order to get the resolution required we focused the laser beam source down to a spot-size of 6  $\mu\text{m}$ . We used a PC running appropriate software to automate the data acquisition. See Appendix III for the Labview™ program.

The normalized open-aperture transmittance z-scan is

$$T(z, s=1) = \sum_{m=0}^{\infty} \frac{[-q_0(z)]^m}{(m+1)^{3/2}} \text{ for } |q_0| < 1, \text{ where} \quad (8)$$

$$q_0(z) = \frac{\beta I_0 L_{\text{eff}}}{\left(1 + \frac{z^2}{z_0^2}\right)}, \quad L_{\text{eff}} = (1 - \exp(-\alpha L)) / \alpha, \quad z_0 = \pi w_0^2 / \lambda, \quad (9)$$

$\alpha$  is the linear absorption coefficient,  $\beta$  is the two photon absorption (2PA) nonlinear saturation of absorption,  $I_0$  is the open aperture peak irradiance,  $w_0$  is the beam waist,  $L$  is the sample thickness, and  $\lambda$  is the wavelength.[15] Using these relationships we determined the nonlinear absorption,  $\beta$ , by numerical evaluation.

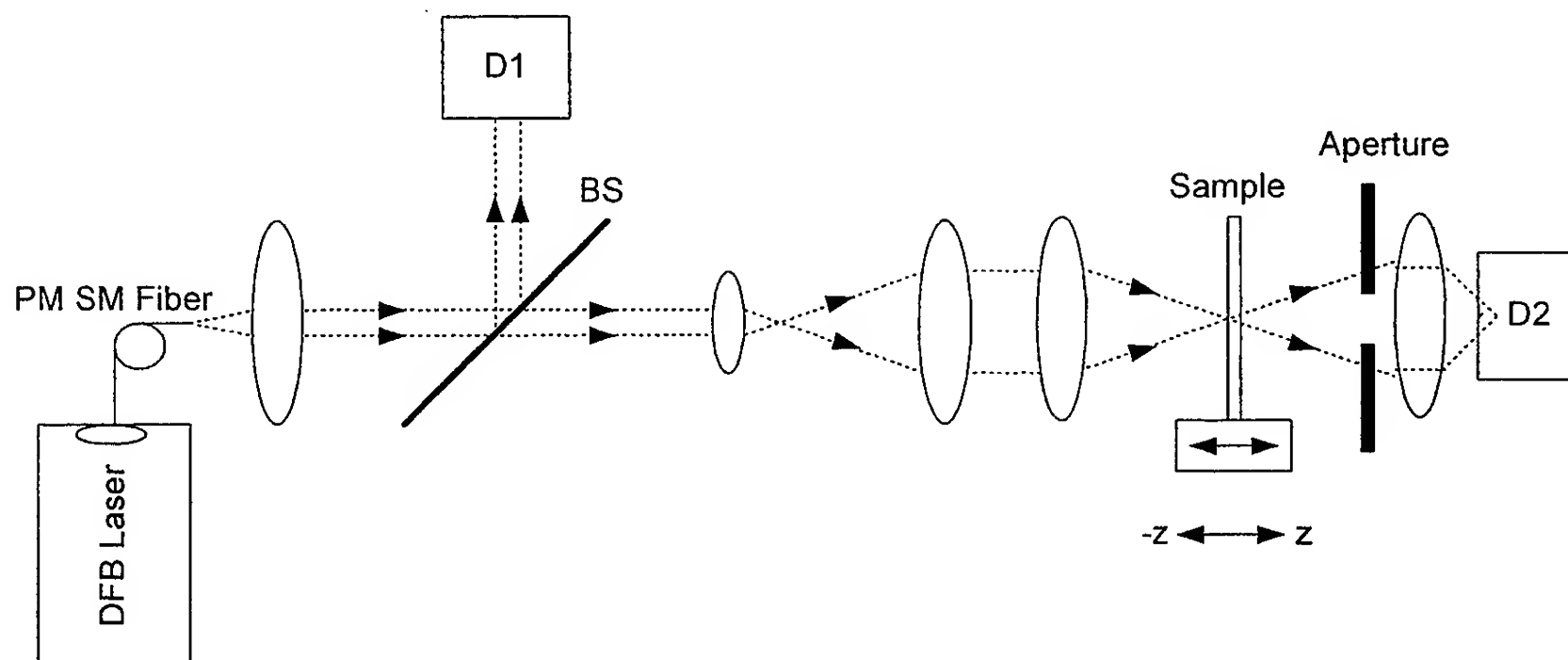


Figure 11. Z-scan set-up for measuring saturable absorbers.

The refractive nonlinear index in saturable absorber material is more difficult to extract since the z-scan output is dominated by the saturation of absorption. A thorough numerical evaluation done by Sheik-Bahae indicated that the nonlinear refractive index was determined within less than 10% uncertainty provided that  $q_0(0) \leq 1$  and  $|\beta/2k\gamma| \leq 1$ . [15] The second condition is met when  $\text{Re}(\chi^{(3)})$  is larger than  $\text{Im}(\chi^{(3)})$  or in other words when the nonlinear refraction dominates over the nonlinear saturation of absorption. For cubic nonlinearity the

index of refraction is expressed in terms of nonlinear indices  $n_2$  (esu) or  $\gamma$  ( $\text{m}^2/\text{W}$ ) through

$$n = n_0 + \frac{n_2}{2}|E|^2 = n_0 + \gamma I, \quad (10)$$

where  $n_0$  is the linear index of refraction,  $E$  is the peak electric field (cgs), and  $I$  represents the irradiance (MKS) of the laser beam within the sample.[15] The refractive nonlinearity can be determined by dividing the closed aperture normalized z-scan by the open aperture normalized z-scan. The result is a new z-scan where  $\Delta T_{p-v}$  agrees within 10% of that obtained from a purely refractive z-scan, given that the two conditions mentioned above are satisfied. From this result the refractive nonlinearity can be calculated by the following relation

$$\gamma = \frac{\Delta T_{p-v}}{0.406 k L_{\text{eff}} I_0 (1-s)^{0.25}} \quad (11)$$

where  $\Delta T_{p-v}$  is the difference between the peak and valley closed/open normalized z-scan,  $S$  is the aperture linear transmittance,  $k=2\pi/\lambda$ , and  $I_0$  is the on-axis irradiance at the focus.[15]

In Figure 12, we show a plot of the normalized Z-scan. From the open aperture case, we were able to determine the nonlinear absorption,  $\beta$ , of  $-1.1 \text{ cm/W}$ . The solid line is the closed aperture case divided by the open aperture case. From this normalized plot, we were able to determine the nonlinear refractive index,  $\gamma$ , as  $-4.0 \times 10^{-6} \text{ cm}^2/\text{W}$ . The relation  $\beta/2k\gamma$  was  $-3.4$  and therefore did not satisfy the relation required to determine the refractive nonlinearity within less than 10% uncertainty. The terms  $n_2$  and  $\gamma$  are related through the following conversion formula  $n_2 = (cn_0/40\pi)\gamma$  in  $\text{m}^3/(\text{watt-sec})$  or esu, where  $c$  is the speed of light in a vacuum.[15]

In Figure 13, we compared the absolute z-scan transmittance of a number of MQW saturable absorbers. The quantum well region of the samples consisted of 50 periods 100 Å InGaAs wells and 100 Å InAlAs barriers on an InP substrate, except #1948 which consisted of 75 periods of 80 Å InGaAs and 100 Å InAlAs. The wavelength of the source was 1549 nm. The

absolute transmittance is calculated by dividing the optical power transmitted through the sample ( $P_s$ ) divided by the optical power transmitted through free space ( $P_{fs} = 2.1 \text{ mW}$ ). We found the transmittance to range from 0.25 to 0.5. The higher the peak the more saturation of absorption. Figure 14 shows that sample #1948 had the highest saturation of absorption and sample #1442 had the lowest. From the plotted normalized transmittance we calculated the absorption coefficient,  $\beta$ , of each of the samples. Using equations 8 and 9, we determined  $\beta$ s of  $-2.5 \text{ cm/W}$ ,  $-2.9 \text{ cm/W}$ ,  $-1.8 \text{ cm/W}$ ,  $-1.1 \text{ cm/W}$ , and  $-1.0 \text{ cm/W}$  for sample #s 1948, 1590, 1643, unknown, and 1442, respectively. Figure 15 shows the absolute z-scan transmittance of a  $500 \text{ }\mu\text{m}$  InP substrate. The InP substrate thickness was much larger than the Raleigh range of the laser ( $z_0$ ) and therefore one cannot use the thin sample relationships to calculate the nonlinear effects.

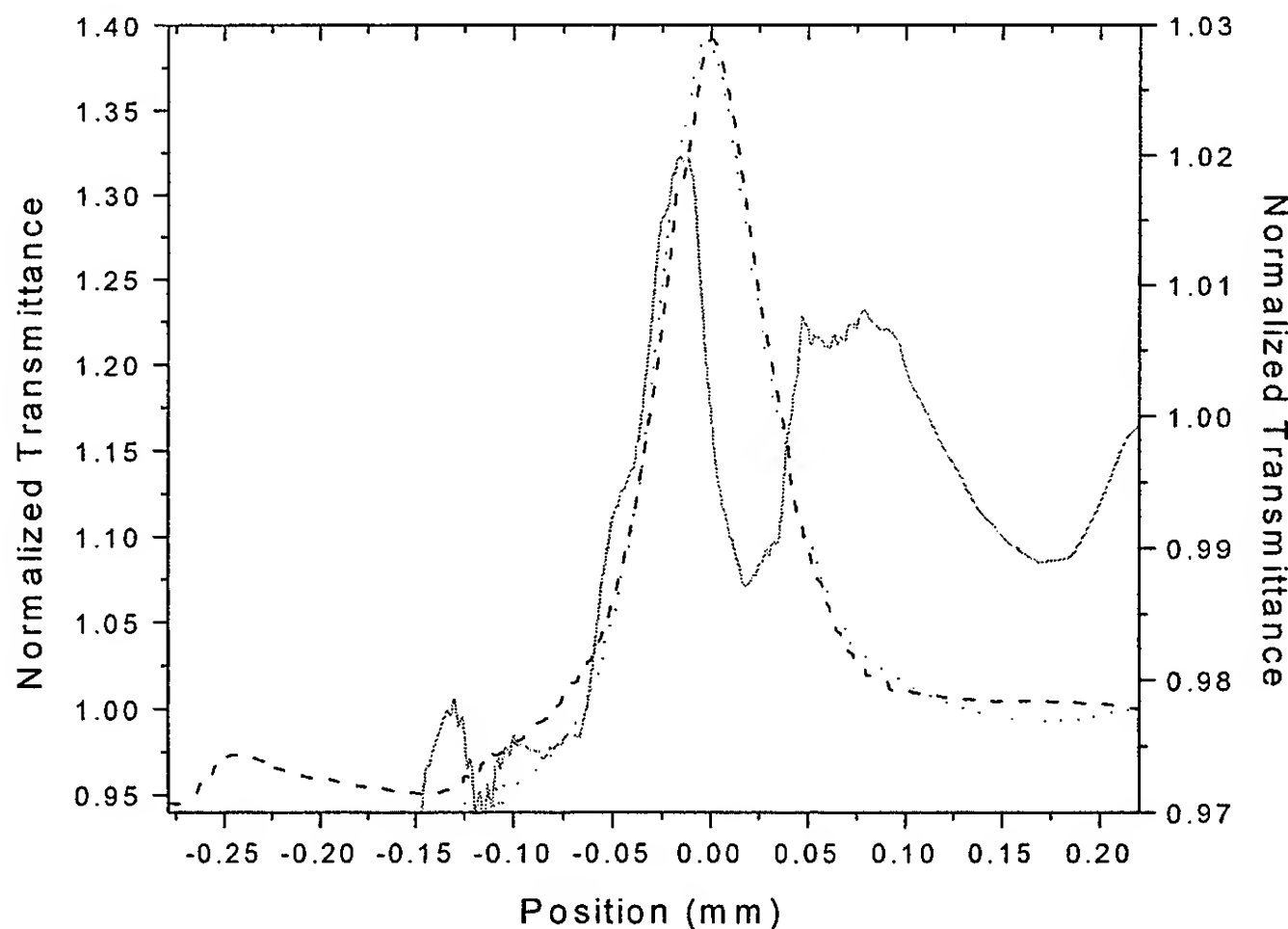


Figure 12. Z-scan of saturable absorber #1590. The dashed line is the normalized transmittance for the open aperture case and the dotted line is for the closed aperture case (at 50% transmittance or  $S=0.5$ ). From the open aperture case, we were able to determine the nonlinear absorption,  $\beta$ , of  $-1.7 \text{ cm/W}$ . The solid line is the closed aperture case divided by the open aperture case. From this normalized plot, we were able to determine the nonlinear refractive index,  $\gamma$ , as  $-4.0 \times 10^{-6} \text{ cm}^2/\text{W}$ .

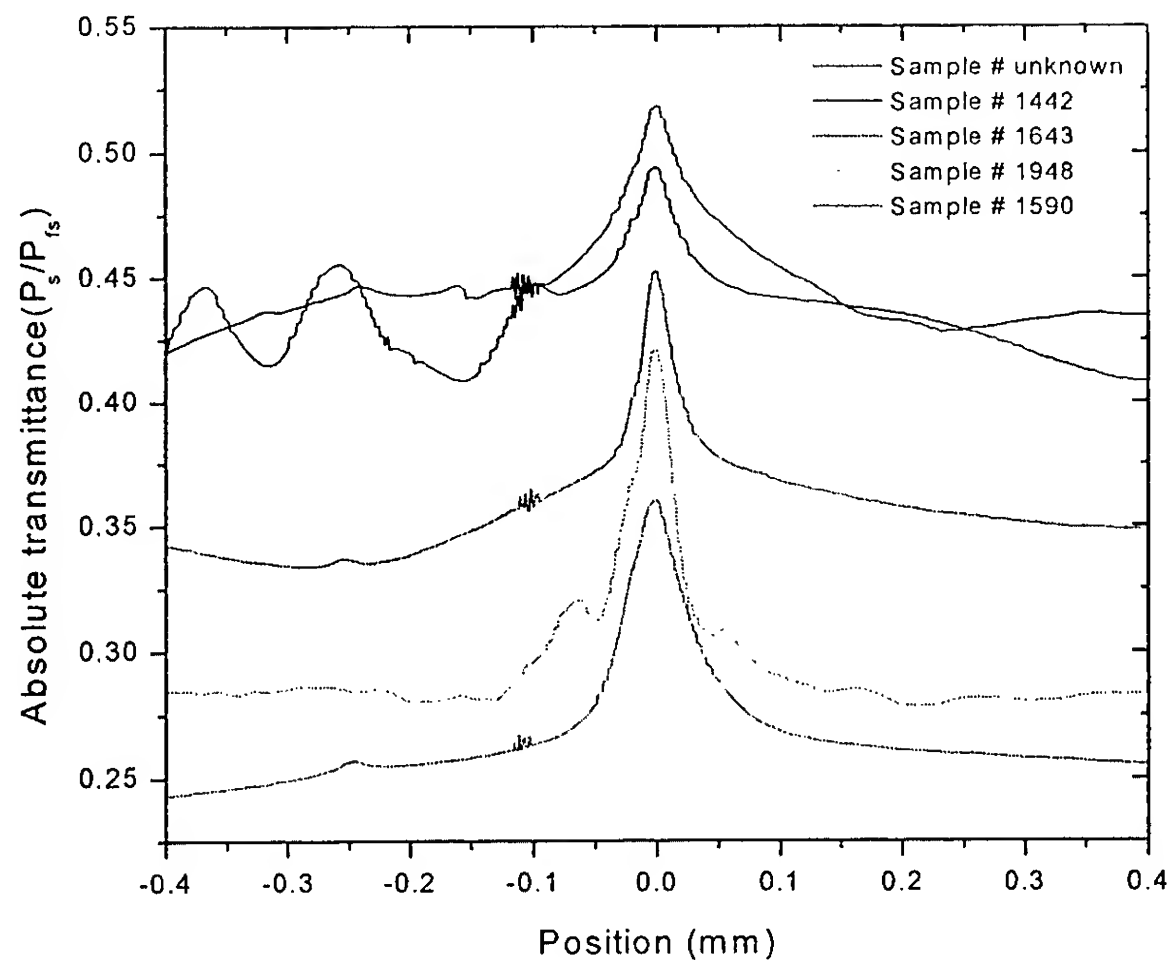


Figure 13. This plot shows the absolute transmittance open aperture z-scan of a number of different multiple quantum well saturable absorbers. The samples are listed from highest to lowest transmittance

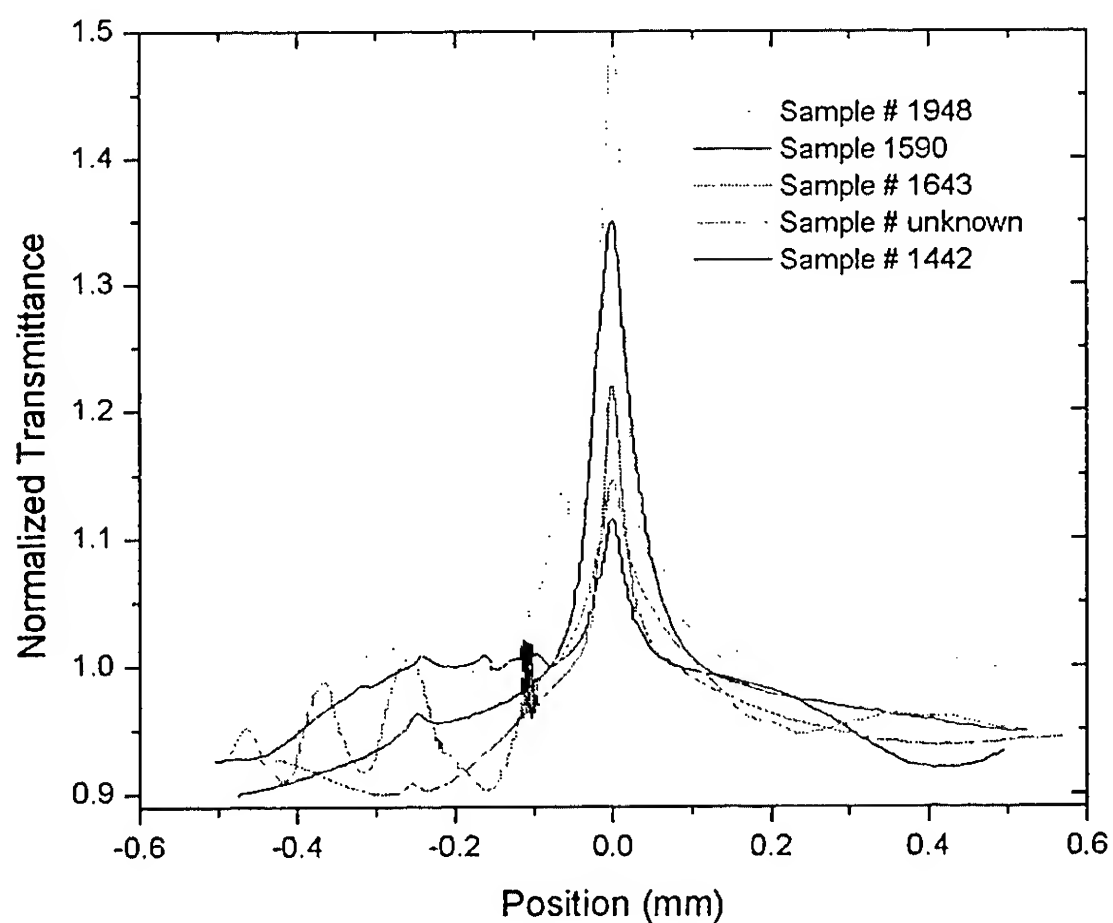


Figure 14. This plot shows the normalized transmittance of a number of different multiple quantum well saturable absorbers 1.00 to 1.35  $\mu\text{m}$  thick. The samples are listed from highest to lowest normalized transmittance

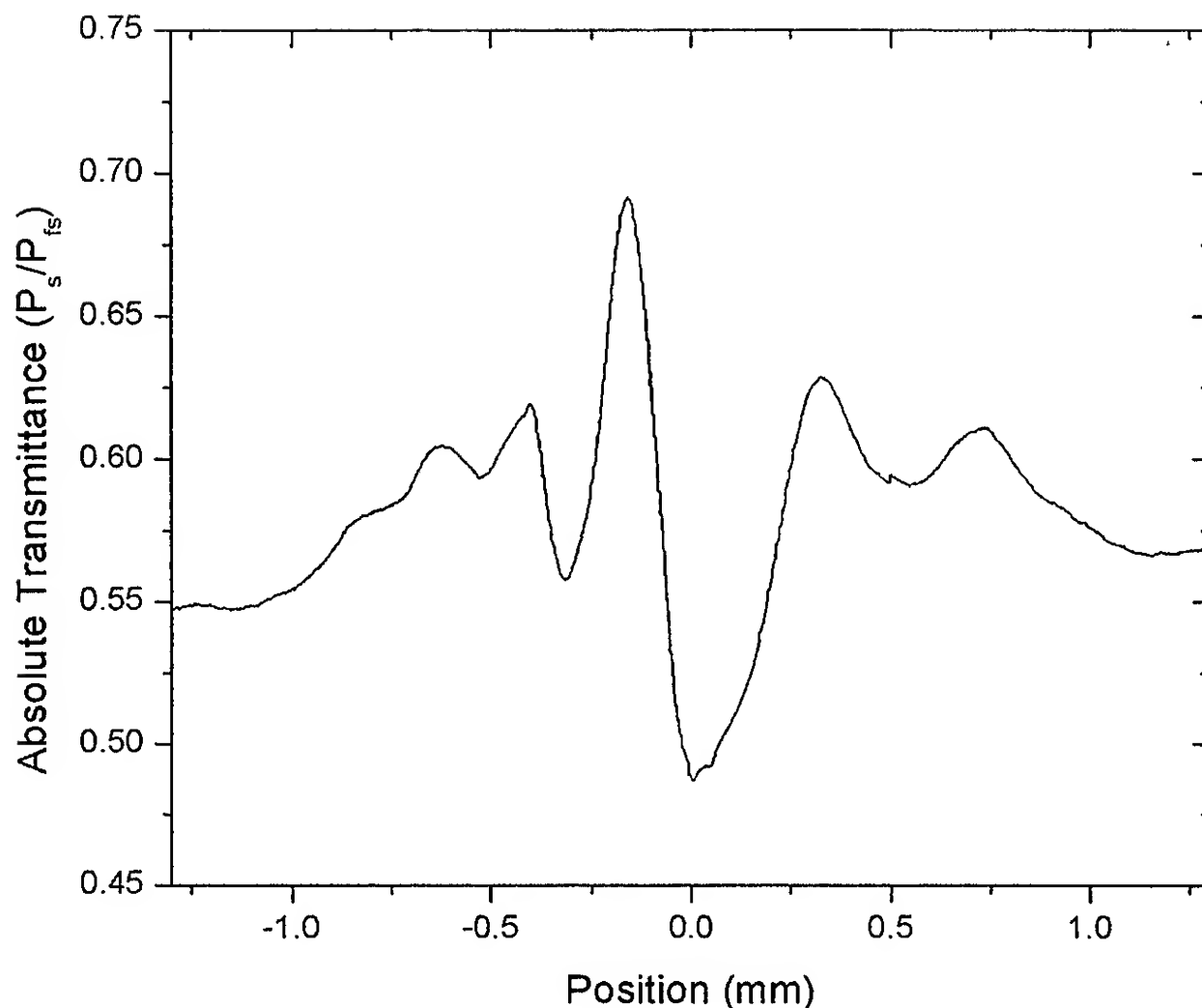


Figure 15. This is the absolute z-scan transmittance of a 500  $\mu\text{m}$  InP substrate. The InP substrate thickness was much larger than the Raleigh range of the laser ( $z_0$ ) and therefore one cannot use the same relationships to calculate the nonlinear effects of the substrate alone.

## 5. Conclusions

A mode-locked fiber laser design incorporating a MQW saturable absorber and a chirped fiber Bragg grating is reliably mode-locked with pulse widths as short as 2 ps. No polarization control in the cavity is required. The dispersion in the cavity and the nonlinearity of the MQW saturable absorber was measured. The dispersion and nonlinearity measurements can be used to simulate the mode-locked operation of the laser. Our fiber dispersion measurements were consistent with published values, but there was some variability due to the stability of the interference measurements and the limited spectral range of our source. Koch *et. al* used a super-continuum fiber laser with a much higher signal to noise ratio over a very wide spectrum,

allowing for measurements over the entire spectral range from 1.1  $\mu\text{m}$  to 1.7 $\mu\text{m}$ . [14] Koch *et al.* also used two broad-band 3dB fused couplers instead of the bulk beam-splitters and mirrors to simplify alignment and to increase stability. [14] The measured dispersion of different fiber Bragg gratings was consistent with the type of gratings, but there were some fluctuations inherent in the tunable laser. These periodic fluctuations in the reflectivity measurements and the dispersion measurements were most likely due to the etalon effects within the tunable laser source. The 0.1-nm FWHM tunable laser was adequate for our purposes, since the spectral bandwidth of the mode-locked fiber laser was about 1 nm FWHM. If finer dispersion measurements are required, a more stable and narrower linewidth tunable laser source must be used. [9,12]

The nonlinearity results were consistent with MQW structures determined with different methods in other papers. [16] The absorptive nonlinearity can be determined fairly easily using this technique. The refractive nonlinearity was much more difficult to determine due to the strong absorptive nonlinearity, but the sign of the refractive nonlinearity and the order of magnitude was easily determined. Some sources of error in our measurements would be due to our lack of an accurate measurement of the spot size of the laser. We estimated the spot size of the laser to be approximately 6  $\mu\text{m}$  referenced to the  $e^{-2}$  power points. A more accurate characterization of the beam and spot size would lend more confidence to the measurements. In addition, a measurement of known reference material would allow us to calibrate the z-scan set-up. There was also some variability in the saturation of absorption depending upon where in the x-y plane of the MQW the laser was focused. Finally, there could have been some errors because we are measuring a compound structure of the multiple quantum well stack and the InP substrate.

## 6. References

1. M. J. Hayduk, R. J. Bussjager, M. A. Getbehead, and J. A. Louthain, "Recent advancements in photonic converters," Proceedings of the SPIE, San Diego, CA, July 2000.
2. S. Tsuda, W. H. Knox, S. T. Cundiff, W. Y. Jan, and J. E. Cunningham, "Mode-locking ultrafast solid-state lasers with saturable Bragg reflectors," *IEEE J. Sel. Topics Quant. Electr.* **2**, 454-64 (1997)
3. J. N. Kutz, B. C. Collings, K. Bergman, S. Tsuda, S. T. Cundiff, W. H. Knox, P. Holmes and M. Weinstein, "Mode-locking pulse dynamics in a fiber laser with a saturable Bragg reflector," *J. Opt. Soc. Amer. B* **14**, 2681-90 (1997).
4. B. C. Collings, K. Bergman, S. T. Cundiff, S. Tsuda, J. N. Kutz, J. E. Cunningham, W. Y. Jan, M. Koch, and W. H. Knox, "Short Cavity Erbium/Ytterbium Fiber Lasers Mode-Locked with a Saturable Bragg Reflector," *IEEE Journal of Selected Topics in Quantum Electronics*, **3** (4), pp. 1065-1075, 1997.
5. J. W. Haus, M. Hayduk, W. Kaechele, G. Shaulov, J. Theimer, K. Teegarden, G. Wicks, "A mode-locked fiber laser with a chirped Bragg grating," *Optics Communications*, **174**, pp. 205-214, 2000.
6. J.A. Louthain, M. J. Hayduk, and J. W. Haus, "Characterization and modeling of a dispersive cavity mode-locked erbium-doped fiber laser," Conference on Lasers and Electro-optics 2000 sponsored by IEEE/Lasers and Electro-Optics Society and Optical Society of America, CLEO 2000 Technical Digest, May 2000
7. M. J. Hayduk, M. F. Krol, C. R. Pollock, K. J. Teegarden, G. W. Wicks, and W. Kaechele, "Passively mode-locked picosecond erbium-doped fiber lasers using multiple quantum well saturable absorbers," *SPIE Conference on Photonic Processing Technology and Applications II*, **3384**, pp. 2-11, 1998.
8. T. F. Carruthers, I. N. Duling III, M. Horowitz, and C. R. Menyuk, "Dispersion management in a harmonically mode-locked fiber soliton laser," *Optics Letters*, **25** (3), pp. 153-155, 2000.
9. J.A. Louthain, M. J. Hayduk, R. Erdmann, "Dispersion measurements of mode-locked fiber laser components," Proceedings of the SPIE Enabling Photonic Technologies for Aerospace Applications II, Vol. 4042, April 2000
10. J. Stone, D. Marcuse, "Direct Measurement of second-order dispersion in short optical fibres using white-light interferometry," *Electronics Letters*, **20** (18), pp. 751-752, 1984.
11. L. G. Cohen, "Comparison of Single-Mode Fiber Dispersion Measurement Techniques," *Journal of Lightwave Technology*, **LT-3** (5), pp. 958-966, 1985.
12. E. Simova, P. Berini, and C. P. Grover, "Spectral Characterization and Chromatic Dispersion Measurements in Fiber Bragg Gratings for Dispersion Compensation," *IEEE Instrumentation and Measurement Technology Conference*, pp. 712-715, IEEE, St. Paul, 1998.
13. Corning Technical Report, "SMF-28<sup>TM</sup> Fiber Product Information," Corning Incorporated, PI1036, 10/99.
14. F. Koch, S. V. Chernikov, and J. R. Taylor, "Dispersion measurement in optical fibres over the entire spectral range from 1.1  $\mu\text{m}$  to 1.7  $\mu\text{m}$ ," *Optics Communications*, **175**, pp. 209-213, 2000.
15. M. Shiek-Bahae, A. A. Said, T. H. Wei, D. J. Hagan, M. J. Soileau, and E. W. Stryland, "Sensitive Measurement of optical nonlinearities Using a Single Beam," *IEEE J. Quantum Electronics*, Vol 26, No. 4, pp. 760-769, April 1990.



16. T. Kanetake, H. Inoue, S. Tanaka, and K. Ishida, "Large nonlinear optical effect in InGaAs/InAlAs multiplequantum well waveguide," *Electronics Letters*, **29 (19)**, pp. 1682-1684, 1993.

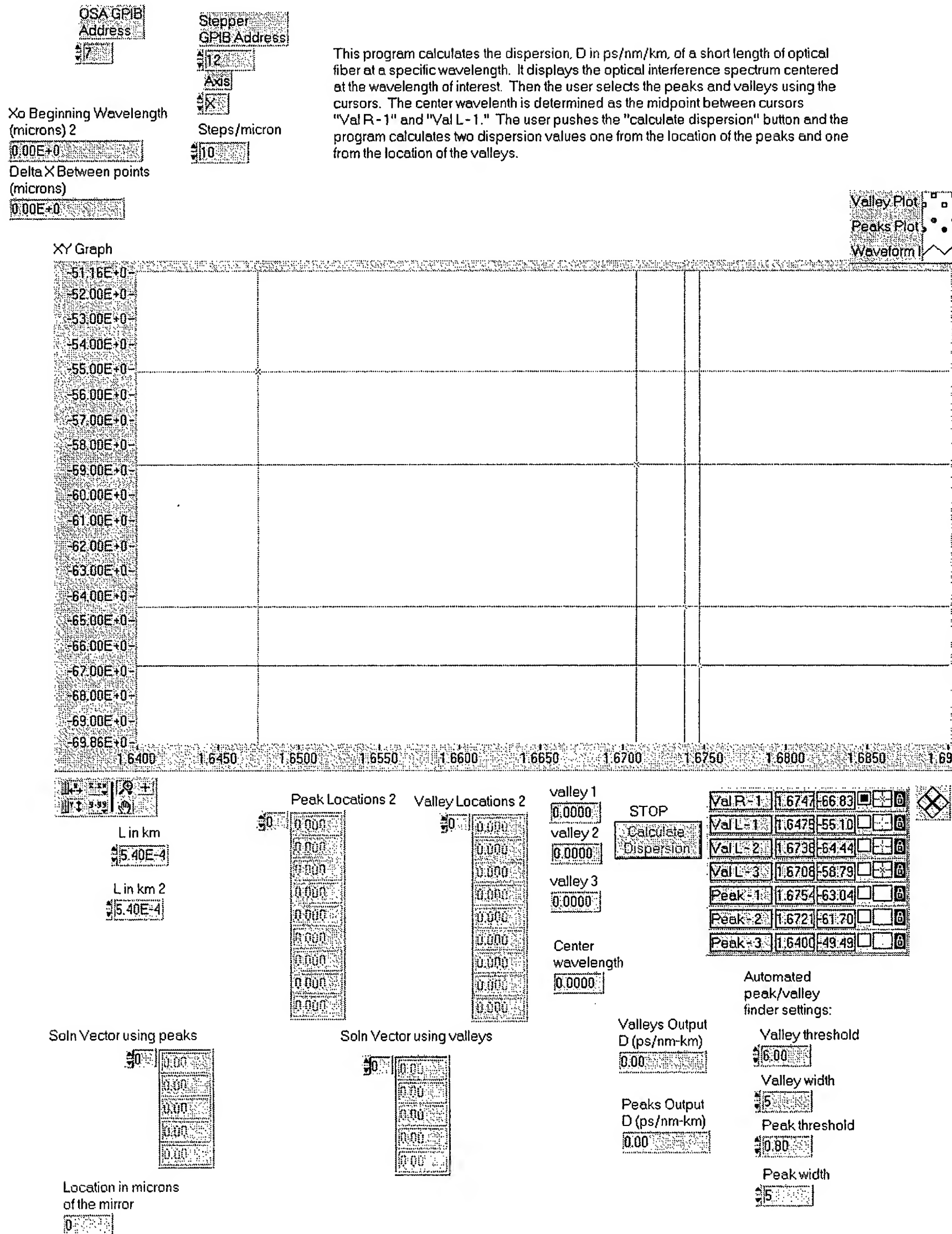
## **7. Acknowledgements**

Numerous people made my work possible. Mike Hayduk designed, built, and characterized the mode-locked fiber lasers. He also designed the multiple quantum well saturable absorbers. Joe Haus designed the model used to simulate the mode-locked lasers. He was also a great resource to ask about measurements and theory. Becky Bussjagger helped me in the lab setting up my experiments. Reinhard Erdmann was a great resource to talk to about measurements and theoretical calculations. Mark Getbehead solved many of my Labview<sup>TM</sup> programming problems.

# Appendix

## I Dispersion Calculation\_linear.vi

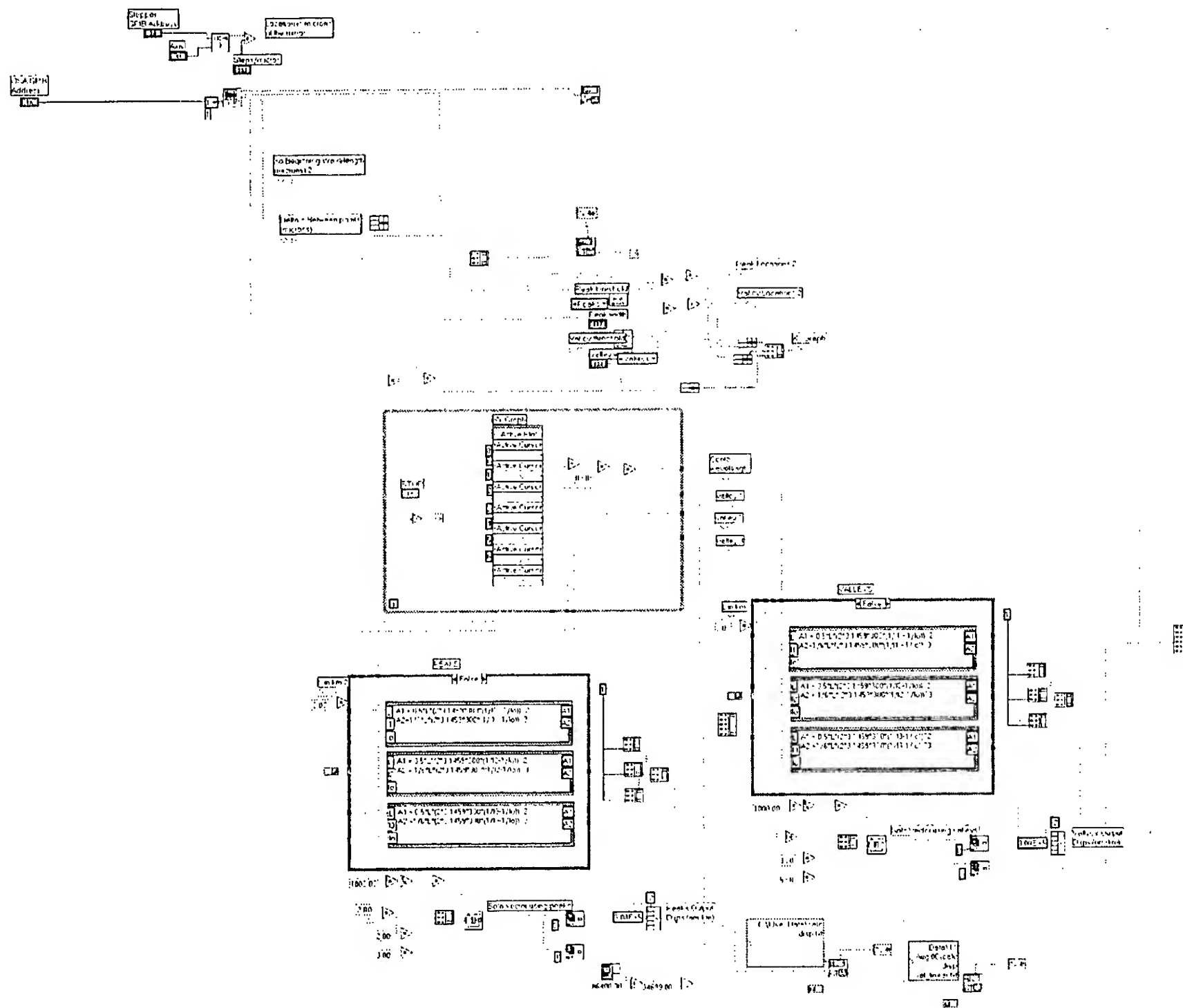
### Front Panel:



## Dispersion Calculation\_linear.vi Program Description:

This program calculates the dispersion,  $D$  in ps/nm/km, of a short length of optical fiber at a specific wavelength. It displays the optical interference spectrum centered at the wavelength of interest. Then the user selects the peaks and valleys using the cursors. The user pushes the "calculate dispersion" button and the program calculates two dispersion values one from the location of the peaks and one from the location of the valleys.

## Block Diagram:



## II Sweep Phase Wavelength.vi

### Front Panel

**Sweep Example**

Start program with above arrow.  
Set parameters and press Start Sweep.  
Laser will reset to the start wavelength then sweep to the stop wavelength.

<b>StartWavelength</b>	<b>StopWavelength</b>	<b>Start Sweep</b>	error out from tunable laser
1550.00	1560.00		
0.00	0.00	Min	Max

<b>ForwardSlewrate</b>	0.00	Max
0.01		
<b>ReturnSlewrate</b>	0.10	

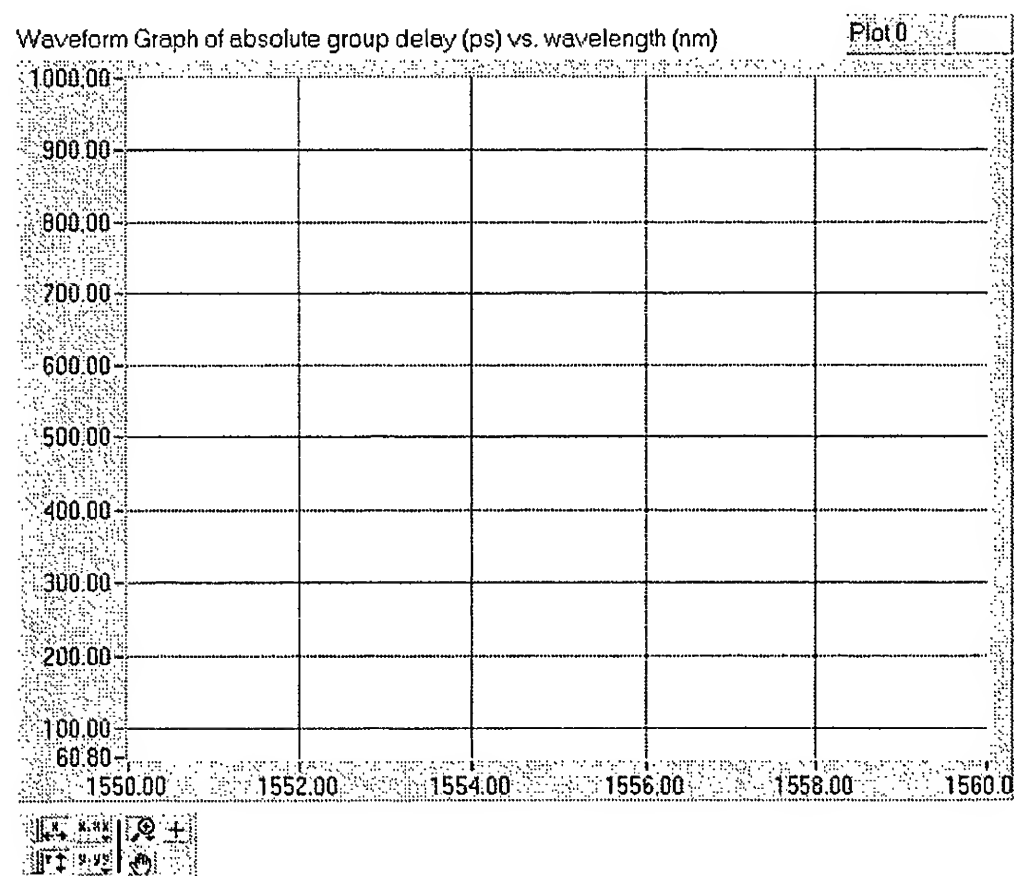
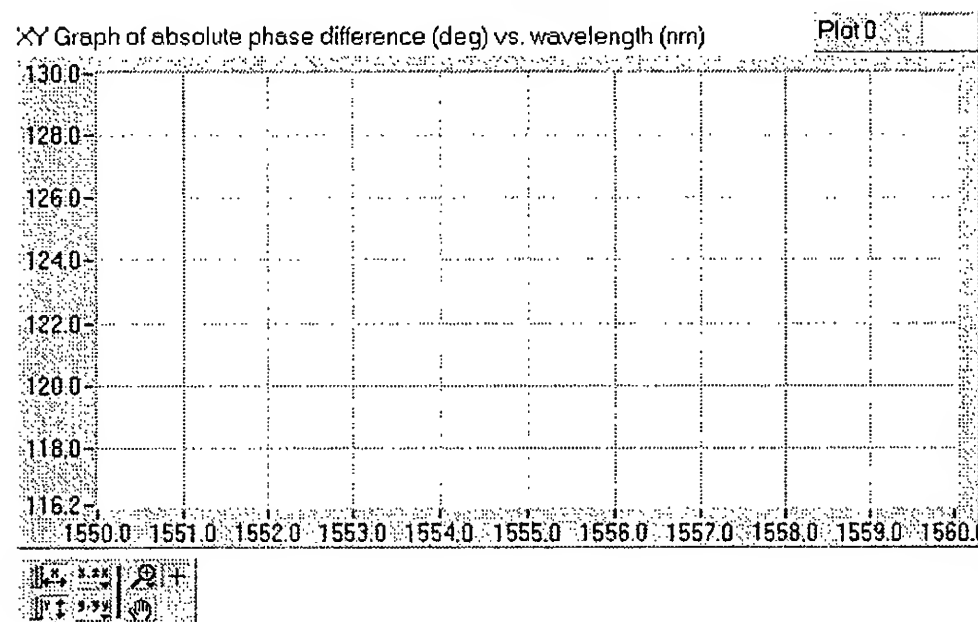
resource name ("")  
gpib:1      GPIB address of tunable laser

error out  
from network analyzer

status	code
OFF	0
source	

Network Analyzer Address      nm/reading      Frequency of Net Analyzer

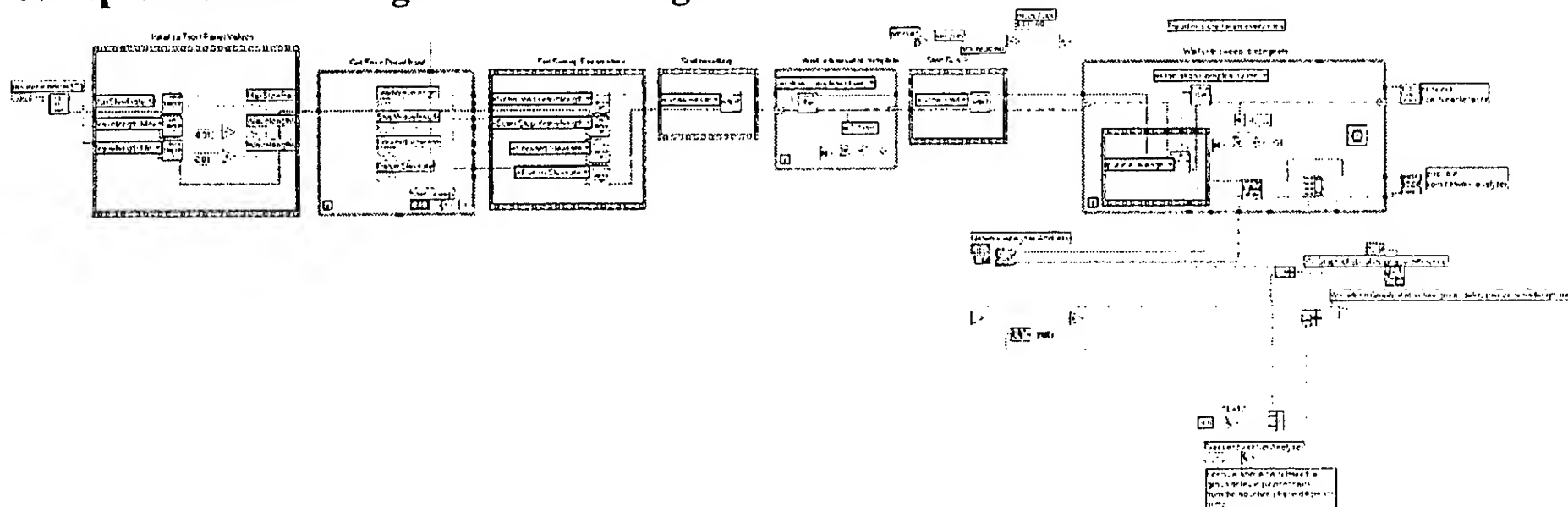
GPIB:16      0.01      100000



## Sweep Phase Wavelength.vi Program Description:

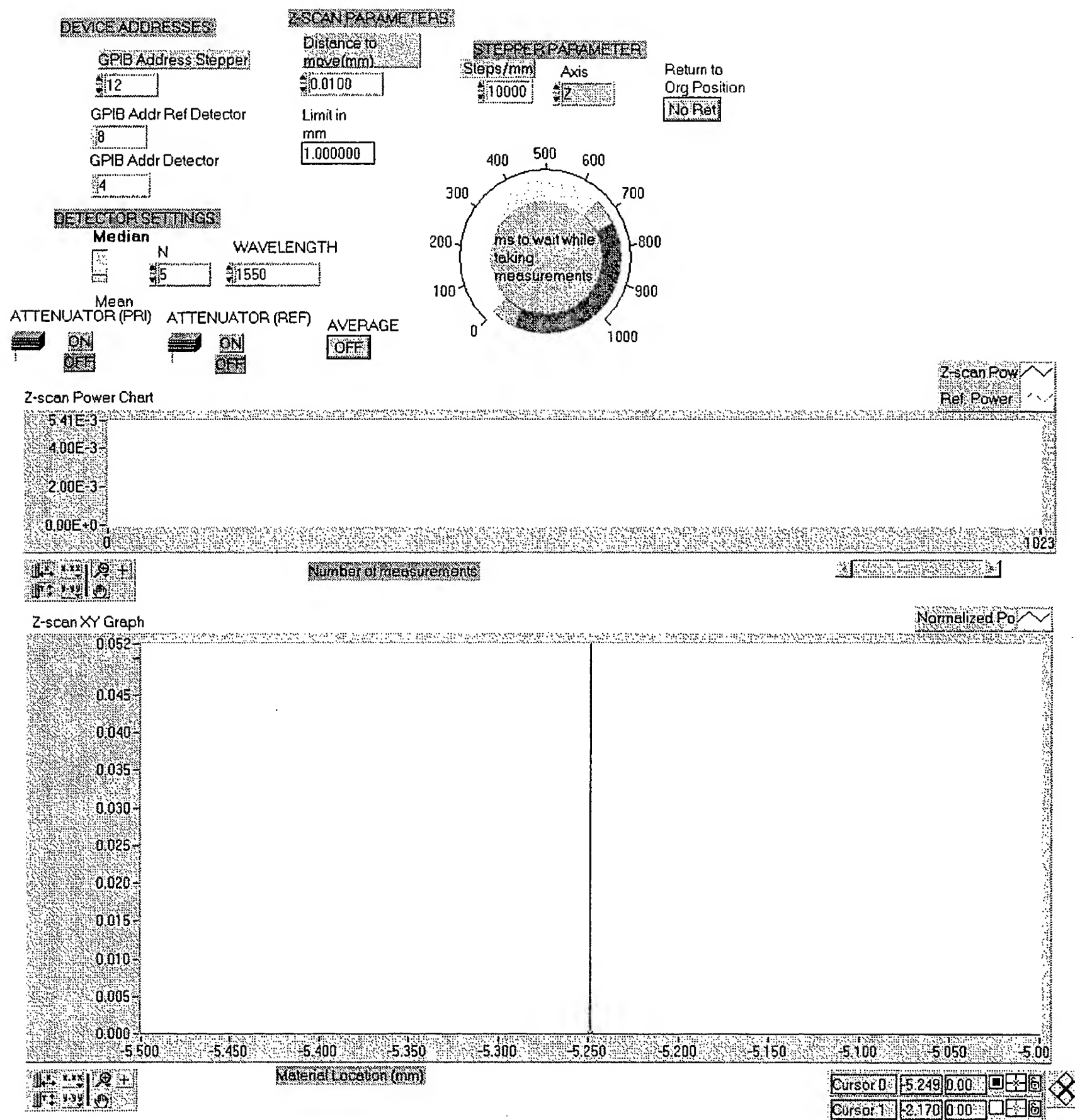
This VI calculates the group delay of a chirped bragg grating versus wavelength. It controls the tunable laser and takes the group delay data from the network analyzer. The network analyzer drives the electro-optic modulator and measures the phase difference after the tunable laser light has reflected back from the chirped bragg grating. It plots the group delay and sends the data to an ASCII file. From the slope of the group delay one can determine the dispersion or the amount of chirp in the grating in (ps/nm)

## Sweep Phase Wavelength.vi Block Diagram:



### III z-scan.vi

#### Front Panel:



#### z-scan.vi Program Description:

This program controls an adjustable stage and takes detector measurements at user specified increments. You can set the detectors to read directly or taken a mean/median of N readings. The information is sent to an ASCII file for further analysis

# z-scan.vi Block Diagram:

